Bull. Chem. Soc. Ethiop. **2022**, 36(4), 815-829.
DOI: https://dx.doi.org/10.4314/bcse.v36i4.8

ISSN 1011-3924
Printed in Ethiopia
Online ISSN 1726-801X

SYNTHESIS, CHARACTERIZATION AND MICROSTRUCTURAL EVALUATION OF ZnO NANOPARTICLES BY WILLIAM-HALL AND SIZE-STRAIN PLOT METHODS

Ghaferah H. Al-Hazmi[1], Mohamed G. El-Desouky[2*] and Ashraf A. El-Bindary[3]

[1]Department of Chemistry, College of Science, Princess Nourah bint Abdulrahman University, P.O. Box 84428, Riyadh 11671, Saudi Arabia
[2]Egyptian Propylene and Polypropylene Company, Port Said 42511, Egypt
[3]Chemistry Department, Faculty of Science, Damietta University, Damietta 34517, Egypt

(Received May 23, 2022; Revised June 24, 2022; Accepted June 24, 2022)

ABSTRACT. At various calcination temperatures 450, 550 and 650 °C, zinc oxide nanoparticles were produced. Calcinated ZnO has high surface area as the BET was 119.12 m^2g^{-1} and the average particle radius was calculated to be 1.16 nm. The dimension of crystallites and straining in ZnO nanoparticles' diffraction peaks remained measured. The Williamson–Hall (W–H) technique besides the size–strain approach stayed used. For each of XRD reflection peaks, physical characteristics like strain and stress were computed. Towards regulate the magnitude of crystallites, the Williamson–Hall (W–H) approach besides the size–strain technique are used that is good agreement with the size that determine from SEM as it was 22.6, 26.6 and 32.6 nm for ZnO calcinated at 450, 550 and 650 °C, individually. Using the W–H plot to modify the subversion shape, assuming an unvarying distortion model (UDM), unvarying stress deformation model (USDM), unvarying deformation energy density model (UDEDM), and The size–strain plan (SSP) approach was used to determine this. The SEM and Scherrer methods match well with the crystal size of ZnO NPs determined using W–H plots and the SSP technique.

KEY WORDS: Zinc oxide nanosphere, Calcination, Physical characterization, W–H investigation, SSP technique

INTRODUCTION

The coloring industry is a large-scale and one of the most important industries across the world. However, due to the range of colours found in its effluent, it is considered a severe source of pollution for species in the environment. Some colours have been proven to be genotoxic [1]. Dysfunction of the kidneys, liver, brain, reproductive functions, and central nervous system are only a few of the human impacts of dyes [2]. As a result, extraction efficiency from the surroundings is a critical factor. Scientists are developing for low-cost solutions to get these dyes out of the water. Textile businesses are thought to emit about 100 tonnes of dyes and pigments into waterways each year [3]. Contaminants can be removed from environmental waterways or sewage using a range of techniques. The majority of them are biological, chemical, or physical purifying methods [4]. Adsorption behavior is the collection of adsorbates by the side of the gas-solid or liquid-solid interface [5, 6]. Van der waal bonds in between adsorbent and the adsorbate make adsorption potentially reversible [7]. Isotherm models are basic principles in the field of adsorption research. They describe how adsorbate and adsorbent react with one another, and they can also be used to compute absorption [7, 8]. Although treatment processes produce unpleasant odours and residues and are costly, adsorption phenomena is appealing for decolorization due to its low cost and flexibility in design, as well as the fact that it does not release any toxic substances after the targeted components have been removed. The main downside of biological therapy approaches is that so many of them take a long time to complete. Most colours, on the other hand, are resistant to physical processes like ion exchange, and electrokinetic coagulation produces a large sludge. Adsorption, on the other hand, is cost-effective, simple to use, and capable of

*Corresponding author. E-mail: ch.moh.gamal@gmail.com

removing nearly all types of impurities. As a result, this method is frequently used to remove not only colours and pigments from waste water and sewage, but also other pollutants such as heavy metal pollutants.

Rivers are by far the most important aspects of the earth's ecology [9]. They transport surface water and nutrients to the oceans through sediment regions. Rivers supply water supply and also aquatic life, that supplies food for both animals and humans. Because of their importance in tourism, hydroelectricity generation, and other industries, rivers are also a valuable resource in modern human society. Regrettably, irresponsible individuals and businesses also exploit waterways as dumping grounds for unwanted goods and chemicals [10]. The primary threat to water security is believed to be direct dumping of pollutants into water bodies from numerous sources without proper treatment. The textile dyeing and processing sector, for example, is ranked as the tenth most industrial pollutants to rivers, contributing 17–20 percent of all industrial water pollution. About 5,000–10,000 tonnes of dyes are discharged into the waterways each year as a result of their widespread use. Congo red (CR) has been one of the most widely used dyes since its beginnings [11]. Once dissolved in water, the molecules of this dye have negative charges, making them anionic dyes. This dye, when released directly into surface waterways, prevents sunlight from penetrating the water (which really is necessary for aquatic plant photosynthesis). It endangers the river environment as well as the local population. As a result, appropriate textile wastewater treatment is essential for ecosystems preservation [12, 13].

Due to its finite size, no crystal is flawless because it would expand in all directions to infinity. The diffraction peaks broaden as a result of the divergence from perfect crystallinity [14]. The two most important properties peak width measurement yields the following results: lattice strain and crystallite size [15]. The dimension of a constructively diffracting domain is measured by crystallite dimensions. The particle size and the particulate crystallite size may not be the same. The percentage of lattice coefficients produced by crystal limitations such as lattice displacements is referred to as lattice strain [15]. Other strain sources have included the triple junction at the grain boundary, contacting or stacking burdens, sinter strains, coherency strains, and other strain causes [16]. Lattice strain and crystallite size could be assessed by means of X-ray profile evaluation, which is a simple yet effective procedure [17]. The pseudo Voigt functionality, rietveld modification, and Warren-Averbach evaluation are three well-known methods for measuring crystallite size and lattice strain [18].

As a result, the W-H technique remains used to evaluate lattice strain and crystallite size in this study. Regardless of the fact that X-ray profile analysis is a standard procedure, it is effective. Apart from SEM micrographs, it remains an unavoidable method of assessing grain size. The average particle size of ZnO nanoparticles as evaluated by direct SEM observations is compared to peak widening (XRD) in this study [19]. A modified variation of W-H was used to calculate the related strain with as-prepared and strengthened ZnO samples at 450 °C due to lattice distortion. The strain caused by the hexagonal crystal's anisotropy is contrasted and displayed against the strain caused by the interplanar gap. In this research, we present quantitatively and qualitatively such observations on ZnO nanoparticles generated by calcination technique.

EXPERIMINTAL

Supplies

All the used substances are established previously [20].

Preparation of the ZnO nanoparticles

The ZnO was obtained by calcination of $[ZnLCl(OH_2)]H_2O$ chelate at temperatures of 450, 550, and 650 ºC for 4 hours. In addition, the dried ZnO sample was sieved with a 200 µm mesh to

obtain small uniform particles. This method produces ZnO nanoparticles quickly and easily, without the use of expensive and harmful solvents or complicated equipment [21].

RESULTS AND DISSCUSION

X-Ray diffraction patterns (XRD)

Figure 1 demonstrates the XRD pattern of ZnO powder [22, 23]. Not any diffraction peaks related to Zn, $Zn(OH)_2$ or additional ZnO stages have been found, ZnO nanoparticles are naturally crystalline, according to the findings. The peaks are sharp and thin, suggesting that the taster is of excellent excellence, with respectable crystallinity and small particle magnitude 17.64, 29.32 and 33.53 nm for calcinated ZnO at 450, 550 and 650 ºC, respectively. The properties of the lattice were computed using XRD data (a = 3.2491 Å and c = 5.2063 Å) [24].

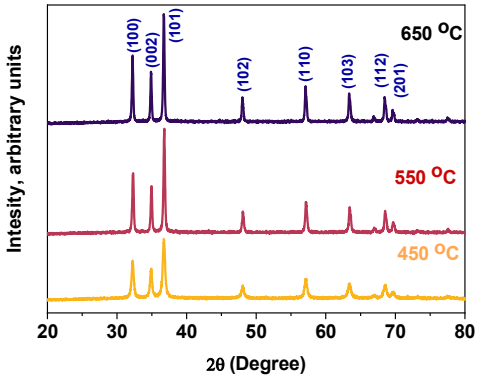

Figure 1. XRD of ZnO at 450, 550, and 650 ºC calcination temperatures.

Determining the size and strain of crystallites

Scherrer method

Spreading of peaks demonstrates grain structure as well as the considerable worded with the powder. The (β_{hkl}) (instrumental broadening) was fixed, Using the connection to associate every ZnO diffraction peak [23, 25]:

$$\beta_{hkl} = [\ (\beta_{hkl})^2_{measured} - \beta^2_{instrumental}]^{1/2} \quad (1)$$

Debye-formula Scherrer's was used to determine the average nanocrystalline size:

$$D = \frac{K\lambda}{\beta \cos\theta} \quad (2)$$

ZnO crystallite size was estimated to be around 17 nm at in height strength peak height at high intensity peak (Table 1).

Williamson–Hall method

Uniform distortion model (UDM). XRD peaks are controlled by a variety of factors, including crystallite size, lattice strain, and structural imperfections in numerous situations. A modified

integral breathing method was used in the Williamson–Hall (W–H) research, whenever the peak breadth is widened as a meaning of 2 theta, it obviously distinguishes the framework size- besides strain-induced distortion highest. The following are distinct contributing to the peak expansion of a Bragg reflection streak:

$$\beta_{hkl} = \beta_S + \beta_D \quad (3)$$

wherever β_{hkl} shows the radiant peak's filled width at half maximum (FWHM), and β_s β_D are the thickness due to the size–strain, correspondingly (Table 1) [15]. Strain is considered constant throughout the crystallographic direction in the W–H equation that is defined by β_{hkl}:

$$\beta_{hkl} = \frac{K\lambda}{D\cos\theta} + 4\varepsilon \tan\theta \quad (4)$$

Reorganizing Eq. (4) provides:

$$\beta_{hkl}\cos\theta = \frac{K\lambda}{D} + 4\varepsilon \tan\theta \quad (5)$$

Here, D and ε resemble to the crystallite size and microstrain values, respectively. By calculating 4 sin theta, the normal size of the crystallites besides the strain may be determined using the Y-intercept extrapolation besides the line's slope understand Figures 1 and 2.

$$D = \frac{K\lambda}{\text{Y Intercept}} \quad (6)$$

$$\varepsilon = \text{Slope} \quad (7)$$

Unvarying stress deformation model (USDM). Within the elastic limit, a linear proportionality relation exists, as per Hooke's law strain (ε) and the stress (σ):

$$\sigma = E\,\varepsilon \quad (8)$$

wherever E is the Young's modulus or elasticity modulus. The equation is a rough estimate that holds true aimed at modest strains. As a result, in the additional component of the calculation denoting UDM, The lattice displacement stress is thought to be uniform and is substituted by ε = (σ/*E*) and Eq. (5) is adjusted as follows:

$$\beta_{hkl}\cos\theta = \frac{K\lambda}{D} + \frac{4\sigma\sin\theta}{Ehkl} \quad (9)$$

E_{hkl} is the plane vertical to the crystal lattice plane's set, Young's modulus (hkl). Using the slope line created between the two axes, the unvarying stress can be designed $4\sigma\sin\theta/E_{hkl}$ and $\beta_{hkl}\cos\theta$, and D is the crystallite size, as illustrated in Figure 3 from the intercept it's possible determined. It is possible to determine the strain if E_{hkl} of hexagonal ZnO nanoparticles is identified. The elastic compliances of materials having a hexagonal crystal stage are related to Young's modulus E_{hkl} as Sij [15]:

$$E_{hkl} = \frac{[h^2 + \frac{(h+2k)^2}{3} + \left(\frac{al}{c}\right)^2]^2}{S_{11}(h^2 + \frac{(h+2k)^2}{3} + S_{33}\left(\frac{al}{c}\right)^4 + (2S_{13} + S_{44})(h^2 + \frac{(h+2k)^2}{3}\left(\frac{al}{c}\right)^2} \quad (10)$$

wherever S_{44}, S_{33}, S_{13}, and S_{11} are the elastic compliances of ZnO, and their standards are 23.57×10^{-12}, 6.940×10^{-12}, 2.206×10^{-12} and 7.858×10^{-12} $m^2.N^{-1}$, individually.

Eq. 10 show the UDSM. Drawing the curve between two axes $\beta_{hkl}\cos\theta$ and $4\sin\theta/E_{hkl}$, Table 1 shows how to compute the uniform deformation stress using the line's slope and lattice strain. Figure 3 shows the USDM for annealed ZnO nanoparticles [15].

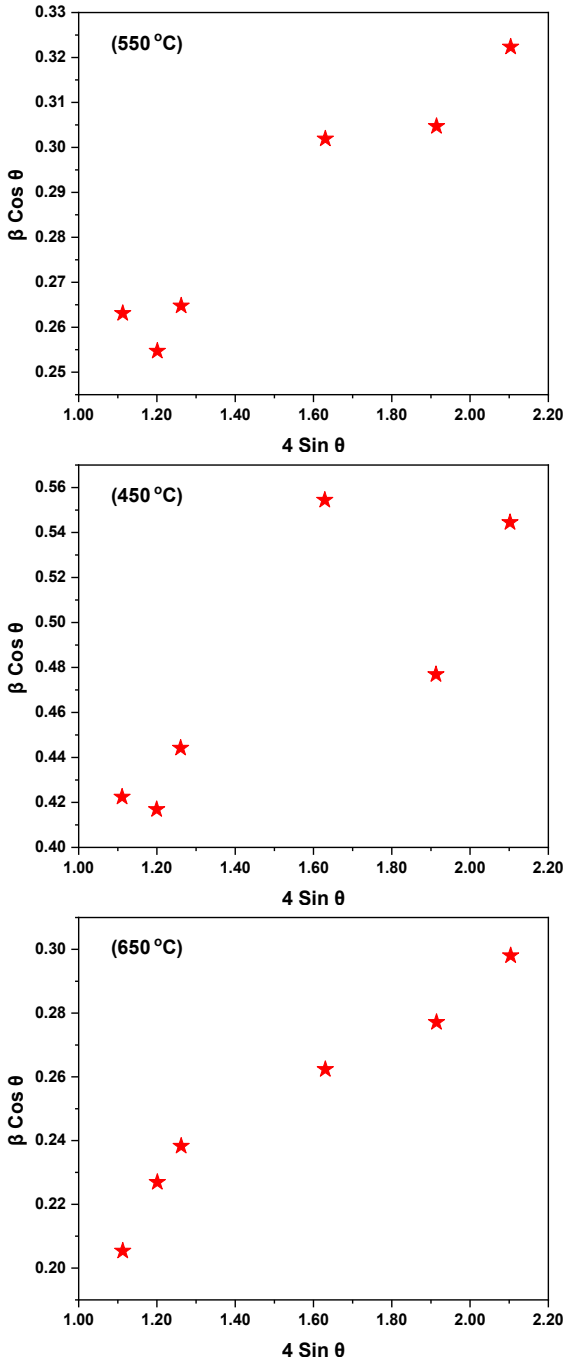

Figure 2. UDM plot for ZnO calcinated at 450, 550, 650 °C.

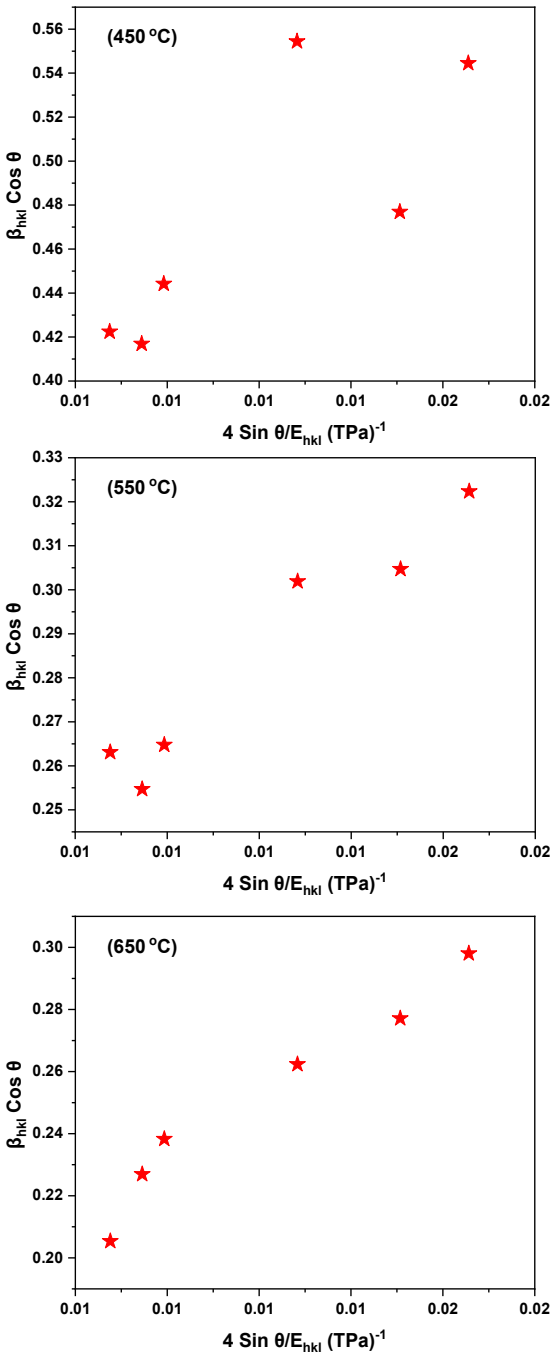

Figure 3. USDM plot for ZnO calcinated at 450, 550 and 650 ºC.

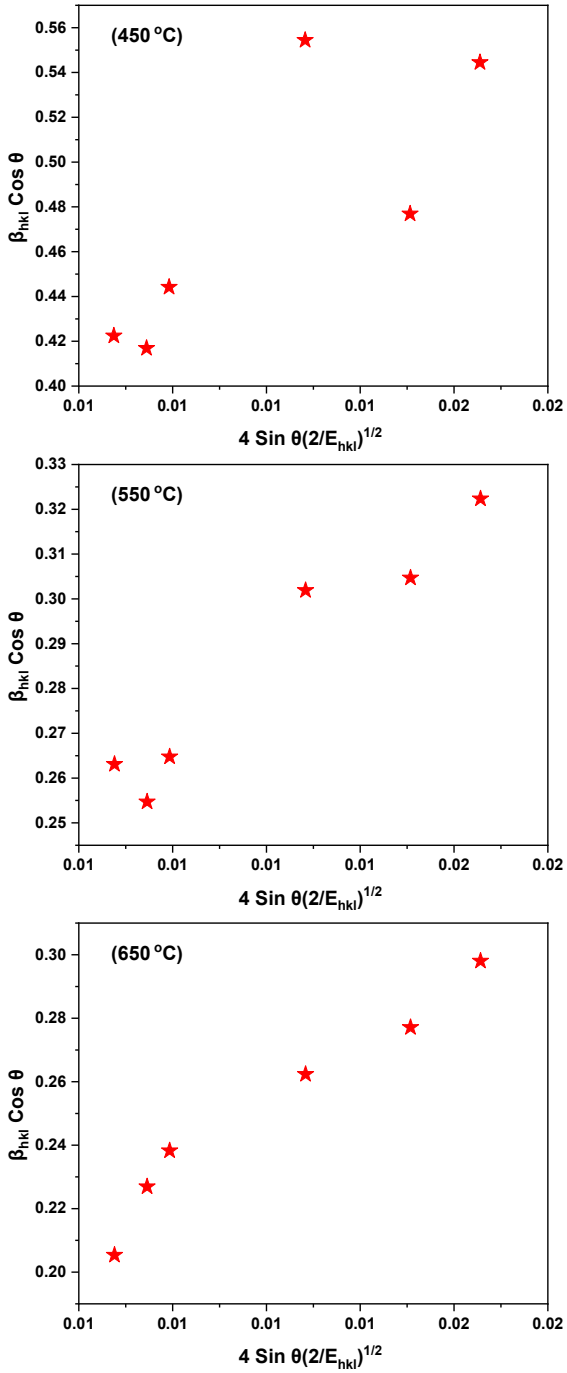

Figure 4. UDEDM plot of ZnO calicinated at 450, 550 and 650 °C.

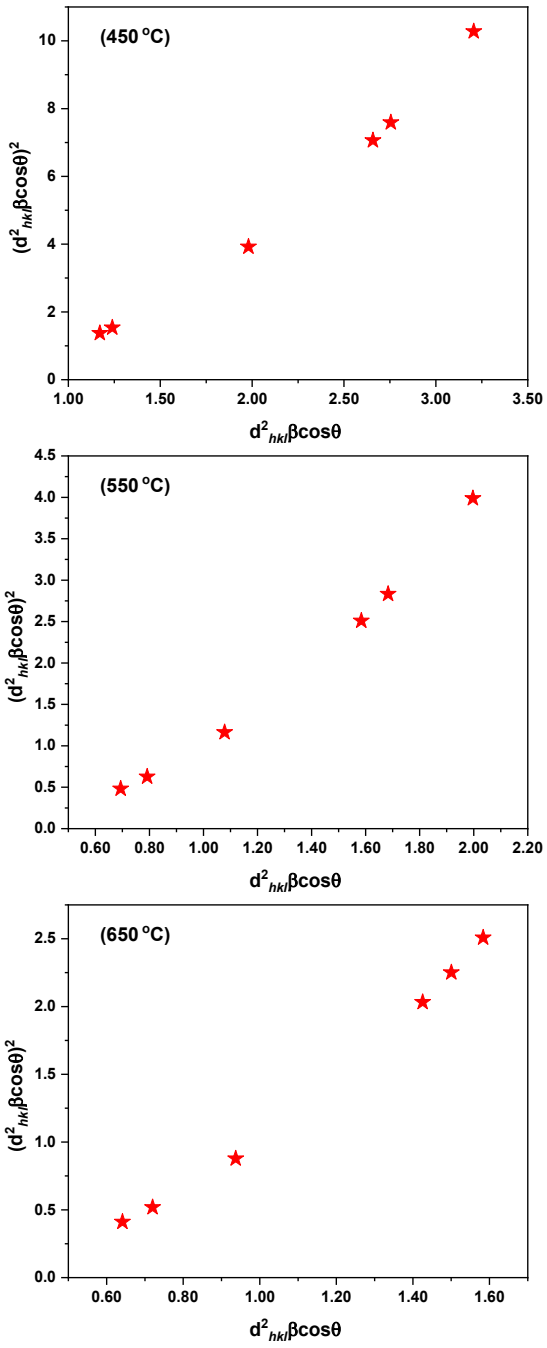

Figure 5. Size-strain plot of ZnO calcinated at 450, 550 and 650 °C.

Unvarying deformation energy density model (UDEDM). UDEDM is a theoretical model for calculating a crystal's energy density. Crystals were previously thought to be isotropic and homogenous. In several cases, the premise of isotropy and homogeneity is not supported. Furthermore, while reviewing the deformation energy density, the proportion coefficients aimed at the strain–stress connection are not broadly distributed (u) (Figure 4). The energy density of an elastic structure obeying Hooke's law (unit energy) could be deduced resulting from the connection $u = (\varepsilon^2 E_{hkl})/2$. As a result, Eq. (11) could be recast using the energy-strain relation [15].

$$\beta_{hkl} \cos\theta = \frac{K\lambda}{D} + (4 \sin\theta \left(\frac{2u}{E_{hkl}}\right)^{1/2}) \quad (11)$$

SSP method

The broadening of the line was virtually isotropic, according to the W–H plot.This suggests that the diffraction fields remained naturally isotropic and that microstrain was a factor.Isotropic line broadening is one type of isotropy, though, a best analysis of the size–strain is possible to gain because high-angle reflections are given an normal "size–strain plot" (SSP), which is less likely to improvement weight and is therefore more accurate. A Lorentz function is thought to describe the "crystalline dimension" characteristic, whereas the "strain profile" is supposed to be defined by a Gaussian function in this technique. As a result, we now have the following (Eq. 12):

$$(d_{hkl}\beta_{hkl} \cos\theta)^2 = \frac{K\lambda}{Dv} + (d^2{}_{hkl}\beta_{hkl} \cos\theta) + \left(\frac{\varepsilon}{2}\right) \quad (12)$$

Identical to W–H approaches, the term $(d_{hkl}\ \beta_{hkl} \cos\theta)^2$ is planned with deference to $d^2_{hkl}\ \beta_{hkl} \cos\theta$ for all ZnO orientation peaks. The slope of the linearly formfitting data determines particle size in this case, and the intercepted root produces strain (Table 1). In Figure 5, the Scherrer formulation, W–H (UDM, USDM, and UDEDM) replicas, and SSP techniques all show that the size of crystallites (D) differs through the calcination temperature [26].

Morphological studies

The structure of ZnO nanoparticles was studied using SEM. As can be observed in the image, the produced nanoparticles are obviously spherical in shape, with approximately groups included in the aggregate of spheres (Figures 6-8). The granulometry spans from 18.76 to 30.3 nm, as shown in micrographs. This agrees well with the findings of the XRD examinations. The average crystallite size of ZnO was measured at various calcined temperatures of $[ZnLCl(OH_2)]H_2O$, Because of the presence of strain in diverse shapes, the average size of crystallites varies slightly. As a result, the average size of crystallites varies slightly. The SSP methodology delivers more appropriate results than the UDM, USDM, and UDEDM approaches, as evidenced by all of the graphs, since the information is additional precisely described in this manner, with completely high-intensity locations contacting linear version [27]. W–H (UDM, USDM, and UDEDM) representations and SSP approaches were used to analyse ZnO nanoparticles utilising X-rays. They concluded that the SSP approach is superior for determining the crystallite size and strain of ZnO nanoparticles. As a result, it is possible to conclude in the present investigation, these models are more accurate. The SSP approach has been shown to be more significant in predicting the crystallite size and straining of ZnO nanoparticles. To determine the size of crystallites and the strain-induced widening caused by lattice deformation, technical parameters of ZnO nanoparticles are given when determining the size and strain of crystallites. The W–H assessment was conducted out using the UDM, UDSM, and UDEDM models, which proved to remain extremely valuable. W–H was formed and developed to measure the size of crystallites as well as to measure the diameter of crystallites in general the elongation inspired deformation caused by network deformation. Dimension estimate and crystallite deformation can be calculated using UDM-based, UDSM, U-DMS, and UDEDM analysis. The XRD powder measurements of

crystallite size and strain correlate well with the SEM outcomes in case of crystallite size and strain. The elastic possessions of the Young S_{ij} (E_{hkl}) module were assessed by the standards of the plane of the lattice (h, k, l). These techniques outlined overhead, such as the size–strain approach, crystal perfection is greatly suggested for evaluating the size distribution of stress, deformation crystals, and energy density values (Table 1) [26].

Table 1. Geometric parameter of ZnO.

Methods		Parameter	Calcination tempearture (°C)		
			450	550	650
Scherrer		D (nm)	17.64	29.32	33.53
Williamson–Hal	UDM	D (nm)	17.85	24.81	31.01
		ε	0.25	0.075	0.11
	USDM	D (nm)	20.22	24.81	28.84
		ε	33.43	10.14	12.91
		σ (MPa)	4245	1288	1639
	UDEDM	D (nm)	20.28	27.6	31.4
		ε	36.6	12.36	14.2
		σ	4648	1570	1803
		U (kJ.m^{-3})	85.62	9.7	12.80
Size–strain		D (nm)	18.6	28.2	32.3
		ε	4.23	2.633	2.229
		σ (MPa)	537.2	334.4	283.1
SEM		D (nm)	22.6	26.6	32.6

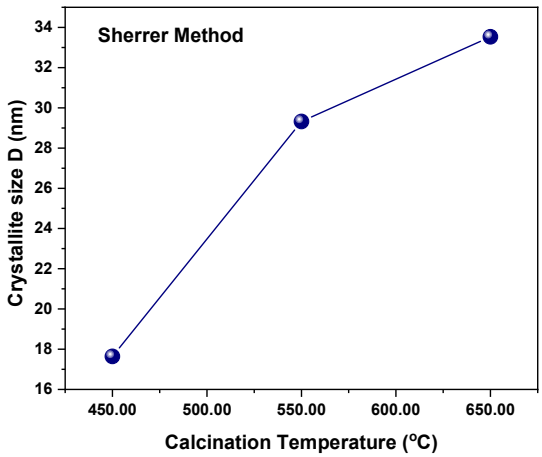

Figure 6. The link among crystallite size (D) and calcination temperature was determined by means of the Scherrer technique.

Brunauer-Emmett-Teller (BET) surface area

The mesoporosity and microporosity lived in this material, as evidenced by the type II pore model. The overall pore volume was 0.362 cm^3g^{-1} and the specific surface area (SBET) was around 119.12 m^2g^{-1}. It showed that the porosity structure of ZnO nanoparticles is good. According with pore distribution, the average particle radius was calculated to be 1.16 nm. The large pore size distribution also enabled for excellent adsorbate molecule inter-diffusion through interconnected, low-resistance channels [28].

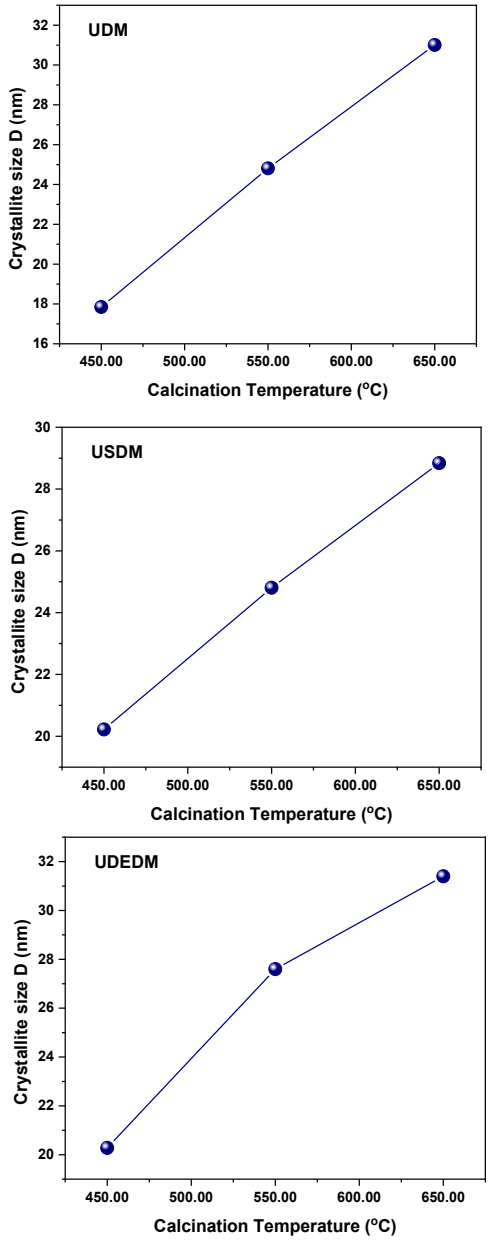

Figure 7. The variation in crystallite size (D) through calcination temperature was determined by means of the W–H technique.

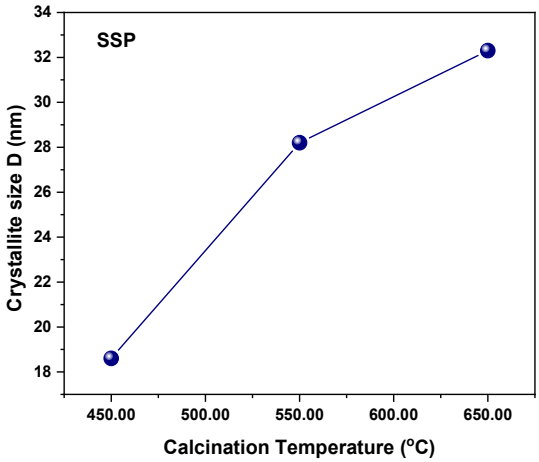

Figure 8. The SSP method was used to determine the variation of crystallite size (D) with calcination temperature.

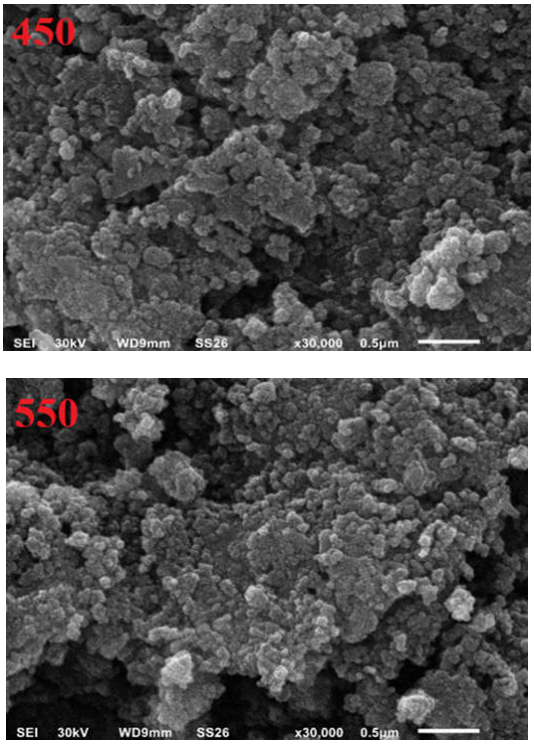

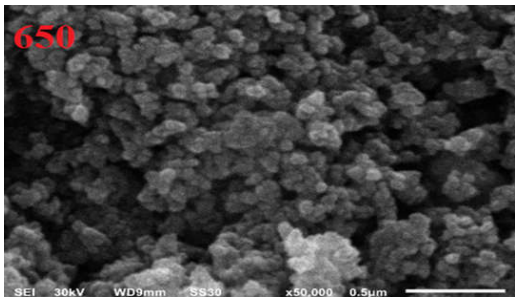

Figure 9. SEM image of ZnO at the calcination temperature of 450, 550 and 650 °C.

SEM analysis

SEM analysis remained used to evaluate the crystalline structure besides morphology of ZnO. The SEM picture of ZnO generated by calcination of ligand at 450 °C is shown in Figure 9. The average diameter of ZnO nanoparticles was roughly 20 nm, which was confirmed by SEM examination. As the calcination temperature rose, the ZnO lengthened [29, 30].

CONCLUSION

The peak line was investigated using the Scherrer formula, the W–H methodology constructed on the UDSM, UDM, and UDEDM replicas, and the SSP technique. The XRD findings of ZnO nanoparticles broaden owing to finite strain and crystallite size. The W–H plot was conceived and designed to measure crystalline nature and strain-induced lengthening owing to lattice distortion. The W–H approach that relies on the UDSM, UDM, and UDEDM models is actual effective in evaluating strain and crystallite size. The W–H was created and established to detect crystallite size and elongation generated distortion due by network distortion. The XRD powder measurements of strain and crystallite size correlate well with the SEM results in terms of crystallite size and strain. The elastic possessions of the Young remained assessed using the parameters of the smooth of the lattice S_{ij} (Ehkl) module (h, k, l). The approaches outlined above, such as the size–strain technique, Crystal perfection is strongly desirable for calculating the regular size of distortion crystals, stress, and energy density value.

ACKNOLOWEDGMENTS

Princess Nourah bint Abdulrahman University Researchers Supporting Project number (PNURSP2022R76), Princess Nourah bint Abdulrahman University, Riyadh, Saudi Arabia.

REFERENCES

1. Bhattacharyya, R.; Ray, S.K. Removal of congo red and methyl violet from water using nano clay filled composite hydrogels of poly acrylic acid and polyethylene glycol. *Chem. Eng. J.* **2015**, 260, 269-283.
2. Vimonses, V.; Jin, B.; Chow, C.W. Insight into removal kinetic and mechanisms of anionic dye by calcined clay materials and lime. *J. Hazard. Mater.* **2010**, 177, 420-427.

3. Han, R.; Ding, D.; Xu, Y.; Zou, W.; Wang, Y.; Li, Y.; Zou, L. Use of rice husk for the adsorption of congo red from aqueous solution in column mode. *Bioresour. Technol.* 2**008**, 99, 2938-2946.
4. Zhu, H.; Jiang, R.; Xiao, L.; Chang, Y.; Guan, Y.; Li, X.; Zeng, G. Photocatalytic decolorization and degradation of Congo Red on innovative crosslinked chitosan/nano-CdS composite catalyst under visible light irradiation. *J.Hazard. Mater.* **2009**, 169, 933-940.
5. Bhaumik, M.; McCrindle, R.; Maity, A. Efficient removal of Congo Red from aqueous solutions by adsorption onto interconnected polypyrrole–polyaniline nanofibres. *Chem. Eng. J.* **2013**, 228, 506-515.
6. Hassan, N.; El-Sonbati, A.; El-Desouky, M. Synthesis, characterization, molecular docking and DNA binding studies of Cu(II), Ni(II), Zn(II) and Mn(II) complexes. *J. Mol. Liq.* **2017**, 242, 293-307.
7. Vijayaraghavan, G.; Shanthakumar, S. Performance study on algal alginate as natural coagulant for the removal of Congo Red dye. *Desalin. Water Treat.* **2016**, 57, 6384-6392.
8. El-Desouky, M.; Abd El-Wahab, M.; El-Bindary, A. Interpretations and DFT calculations for polypropylene/cupper oxide nanosphere. *Biointerf. Res. Appl. Chem.* **2021**, 12, 1134-1147.
9. Vimonses, V.; Lei, S.; Jin, B.; Chow, C.W.; Saint, C. Kinetic study and equilibrium isotherm analysis of Congo Red adsorption by clay materials. *Chem. Eng. J.* **2009**, 148, 354-364.
10. Zhu, H.; Fu, Y.; Jiang, R.; Jiang, J.; Xiao, L.; Zeng, G.; Zhao, S.; Wang, Y. Adsorption removal of Congo Red onto magnetic cellulose/Fe_3O_4/activated carbon composite: Equilibrium, kinetic and thermodynamic studies. *Chem. Eng. J.* **2011**, 173, 494-502.
11. Moradi, S.; Dadfarnia, S.; Haji, A.; Emami, S. Removal of Congo Red from aqueous solution by its sorption onto the metal organic framework MIL-100 (Fe): Equilibrium, kinetic and thermodynamic studies. *Desalin. Water Treat.* **2015**, 56, 709-721.
12. Wu, L.; Liu, Y.; Zhang, L.; Zhao, L. A green-chemical synthetic route to fabricate a lamellar-structured Co/$Co(OH)_2$ nanocomposite exhibiting a high removal ability for organic dye. *Dalton Trans.* **2014**, 43, 5393-5400.
13. El-Bindary, A.; El-Desouky, M.; El-Afify, M. Thermal and spectroscopic studies of some prepared metal complexes and investigation of their potential anticancer and antiviral drug activity against SARS-CoV-2 by molecular docking simulation. *Biointerf. Res. Appl. Chem.* **2021,** 12, 1053-1075.
14. Gul, I.; Maqsood, A.; Naeem, M.; Ashiq, M. Optical, magnetic and electrical investigation of cobalt ferrite nanoparticles synthesized by co-precipitation route. *J. Alloys Compd.* **2010**, 507, 201-206.
15. Irfan, H.; Racik, K.; Anand, S. Microstructural evaluation of $CoAl_2O_4$ nanoparticles by Williamson–Hall and size–strain plot methods. *J. Asian Ceramic Soc.* **2018**, 6, 54-62.
16. Ballarini, N.; Cavani, F.; Passeri, S.; Pesaresi, L.; Lee, A.; Wilson, K. Phenol methylation over nanoparticulate $CoFe_2O_4$ inverse spinel catalysts: The effect of morphology on catalytic performance. *App. Cat. A: Gen.* **2009**, 366, 184-192.
17. Salavati-Niasari M.; Davar F. Synthesis of copper and copper(I) oxide nanoparticles by thermal decomposition of a new precursor. *Mater. Lett.* **2009**, 63, 441-443.
18. Dapiaggi, M.; Geiger, C.; Artioli, G. Microscopic strain in synthetic pyrope-grossular solid solutions determined by synchrotron X-ray powder diffraction at 5 K: The relationship to enthalpy of mixing behavior. *Am. Mineral.* **2005**, 90, 506-509.
19. AlHazmi, G.; AbouMelha, K.; El-Desouky, M.; El-Bindary, A. Effective adsorption of doxorubicin hydrochloride on zirconium metal-organic framework: Equilibrium, kinetic and thermodynamic studies. *J. Mol. Struc.* **2022**, 1258, 132679.
20. El-Desouky, M.; El-Bindary, A.; El-Afify, M.; Hassan, N. Synthesis, characterization, theoretical calculation, DNA binding, molecular docking, anticovid-19 and anticancer chelation studies of some transition metal complexes. *Inorg. Nano-Met. Chem.* **2022**, 521-516.

21. Hassan, N.; El-Sonbati, A.; El-Desouky, M. Synthesis, characterization, molecular docking and DNA binding studies of Cu(II), Ni(II), Zn(II) and Mn(II) complexes. *J. Mol. Liq.* **2017**, 242, 293-307.
22. Altalhi, T.A.; Ibrahim, M.M.; Mersal, G.A.M.; Mahmoud, M.H.H.; Kumeria, T.; El-Desouky, M.G.; El-Bindary, A.A.; Mohamed A. El-Bindary, M.A. Adsorption of doxorubicin hydrochloride onto thermally treated green adsorbent: Equilibrium, kinetic and thermodynamic studies. *J. Mol. Struc.* **2022**, 133160.
23. El-Desouky, M.; El-Bindary, A. Magnetic metal-organic framework (Fe3O4@ZIF-8) nanocomposites for adsorption of anionic dyes from wastewater. *Inorg. Nano-Metal Chem.* **2021**, 1-15.
24. Hassan, N.; Shahat, A.; El-Didamony, A.; El-Desouky, M.G.; El-Bindary, A.A. Mesoporous iron oxide nano spheres for capturing organic dyes from water sources. *J. Mol. Struc.* **2020**, 1217, 128361.
25. Al-Wasidi, A.S.; AlZahrani, I.I.S.; Naglah, A.M.; El-Desouky, M.G.; Khalil, M.A.; El-Bindary, A.A.; El-Bindary, M.A. Effective removal of methylene blue from aqueous solution using metal‐organic framework; modelling analysis, statistical physics treatment and DFT calculations. *ChemistrySelect.* **2021**, 6, 11431-11447.
26. Mote, V.; Purushotham, Y.; Dole, B. Williamson-Hall analysis in estimation of lattice strain in nanometer-sized ZnO particles. *J. Theor.Appl. Phys.* **2012**, 6, 1-8.
27. Zak, A.K.; Majid, W.A.; Abrishami, M.E.; Yousefi, R. X-ray analysis of ZnO nanoparticles by Williamson–Hall and size–strain plot methods. *Solid State Sci.* **2011**, 13, 251-256.
28. El-Desouky, M.G.; El-Bindary, M.A.; El-Bindary, A.A. Effective adsorptive removal of anionic dyes from aqueous solution. *Vietnam J. Chem.* **2021**, 59, 341-361.
29. Hassan, N.; Shahat, A.; El-Didamony, A.; El-Desouky, M.; El-Bindary, A. Equilibrium, kinetic and thermodynamic studies of adsorption of cationic dyes from aqueous solution using ZIF-8. *Moroccan J. Chem.* **2020**, 8, 2627-2637.
30. El-Bindary, M.A.; El-Desouky, M.G.; El-Bindary, A.A. Adsorption of industrial dye from aqueous solutions onto thermally treated green adsorbent: A complete batch system evaluation. *J. Mol. Liq.* **2021**, 117082.